Journal of Hazardous Materials xxx (2009) xxx–xxx

Contents lists available at ScienceDirect

Journal of Hazardous Materials

journal homepage: www.elsevier.com/locate/jhazmat

Photocatalytic decomposition of 4-*t*-octylphenol ~~by~~ $NaBiO_3$ driven by visible light: Catalytic ~~kinetic~~ and ~~corroded product~~ characterization

Xiaofeng Chang[a,b], Jun Huang[a], Cheng Cheng[c], Wei Sha[d], Xue Li[a], Guangbin Ji[b], Shubo Deng[a], Gang Yu[a,*]

[a] POPs Research Center, Department of Environmental Science and Engineering, Tsinghua University, Beijing 100084, PR China
[b] Nanomaterials Research Institute, College of Materials Science and Technology, Nanjing University of Aeronautics and Astronautics, Nanjing 210016, PR China
[c] Department of Materials, Loughborough University, Loughborough, Leicestershire LE11 3TU, United Kingdom
[d] Department of Electrical and Electronic Engineering, University of Hong Kong, Pokfulam Road, Hong Kong

ARTICLE INFO

Article history:
Received 16 June 2009
Received in revised form 31 August 2009
Accepted 31 August 2009
Available online xxx

Keywords:
$NaBiO_3$
Photocatalysis
4-*t*-Octylphenol
BiOCl

ABSTRACT

The photocatalytic decomposition of 4-*t*-octylphenol (4-*t*-OP) by $NaBiO_3$ ~~semiconductor~~ and the catalyst stability in aqueous solution were investigated systematically for the first time. The results showed that some parameters such as catalyst dosage, initial 4-*t*-OP concentration and pH value of the solution had great effects on the photocatalytic activity. The $NaBiO_3$ photocatalyst maintained considerable catalytic performance under visible light ($\lambda > 400$ nm) irradiation and exhibited a higher photocatalytic activity compared to the commercialized photocatalyst P25.

In addition, the ~~corroded~~ products of $NaBiO_3$ catalyst under acid condition (HCl aqueous solution contained) were characterized by X-ray diffraction (XRD), transmittance electronic microscopy (TEM), selected area electron diffraction (SAED), X-ray photoelectron spectroscopy (XPS) and UV–vis transmittance spectrum analysis. The results showed that $NaBiO_3$ was unstable under the acidic condition and the catalyst could convert into Bi^{3+}-containing compounds such as Bi_2O_3, etc. The experiment demonstrates that $NaBiO_3$ can be corroded to nano-sized BiOCl ~~polycrystalline~~ in the presence of hydrogen chloride, the band gap of which was estimated to be 3.28 eV by Tauc's approach.

1. Introduction

4-*t*-Octylphenol (4-*t*-OP), which is a kind of alkylphenols, has been reported to bio-accumulate in the lipids of water organisms [1]. It also belongs to a kind of endocrine disrupting compounds (EDCs) owe to the fact of causing modifications of sexual development and reproductive function in wildlife [2]. In regard to the removal of 4-*t*-OP or other EDCs, TiO_2 photocatalyst has been attempted to photocatalytically decompose these chemicals under ultraviolet light irradiation, since the catalyst have shown some advantages, such as optical-electronic properties, low cost, high photocatalytic activity, chemical stability and non-toxicity [3–6].

However, the photocatalytic activity of TiO_2 in visible light is extremely low due to its wide band gap (3.0–3.2 eV), which is unable to allow efficient absorption of the most sunlight. Thus, the development of visible light-sensitive photocatalysts has received considerable attention to be used as an alternative for treating contaminated water. Previous works demonstrated that the application of oxides of Bi^{3+} (filled with s^2 electronic configuration) can reduce the band gap for visible light absorption and increase the valance band (VB) width providing facile hole mobility, due to the fact that the $6s^2$ ~~orbital's~~ of Bi^{3+} can form the top of valence band (VB) by overlapping with O 2p orbital [7,8]. Several Bi^{3+}-contained photocatalysts have been developed so far, such as $CaBi_2O_4$ [9], Bi_2WO_6 [10,11], etc.

Recently, Choi and coworkers [8] reported that Bi^{5+} played a significant role in modifying the conduction band (CB) of $BaBi_{0.5}{}^{3+}Bi_{0.5}{}^{5+}O_3$ photocatalyst, because it lowered the CB position for visible light absorption and increased the valance band (VB) width which may provide facile hole mobility. $NaBiO_3$ is a new efficient photocatalyst [12] which was firstly reported by Kako et al. Kou et al. [13] investigated the photocatalytic oxidation of polycyclic aromatic hydrocarbons (PAHs) over $NaBiO_3$ under visible light irradiation. Their results showed that $NaBiO_3$ presented an efficient degradation towards the organic compounds. However, there are still some questions that have not been answered. The photocatalytic kinetics and the water stability of $NaBiO_3$ photocatalyst are still unknown and relevant results have not been published, both of which are essential in the application of waste water treatment. In the present study, we systematically evaluated the effects of catalyst dosage, initial concentration and pH value

* Corresponding author. Tel.: +86 10 6278 7137; fax: +86 10 6279 4006.
E-mail addresses: huangjun@tsinghua.edu.cn (J. Huang), yg-den@tsinghua.edu.cn (G. Yu).

0304-3894/$ – see front matter © 2009 Published by Elsevier B.V.
doi:10.1016/j.jhazmat.2009.08.148

of the pollutant solution on the photocatalytic kinetics of 4-*t*-OP in the presence of $NaBiO_3$ under visible light ($\lambda > 400$ nm) irradiation. Furthermore, the stability of such catalyst in acid solution (HCl aqueous solution contained) after photocatalytic reaction was investigated.

2. Experimental

2.1. Materials

Analytical grade 4-*t*-OP was provided by TCI (Japan). Methanol and acetonitrile are both high performance liquid chromatography (HPLC) grade, obtained from Fisher Chemicals (USA). TiO_2 (product name P25, particle diameter 30 nm, surface area 50 $m^2\,g^{-1}$) was provided by Degussa Company (Germany). $NaBiO_3$ catalyst, hydrochloric acid and sodium hydroxide were analytical reagent grade from Sinopharm Chemical Regent Co., Ltd. All chemicals were used without further purification. Ultrapure (Milli-Q) water was used in the present work. In order to improve the solubility of 4-*t*-OP, 30% methanol was added into the aqueous solution.

2.2. Methods

2.2.1. Photocatalytic kinetics studies

The photocatalysis experiment was carried out in an XPA-Photochemical Reactor (Xujiang Electromechanical Plant, Nanjing, China). The photocatalytic reactor consists of two parts: a 250-mL quartz glass reactor and a Xenon-lamp (power = 500 W) which was parallel to the reactor. 2 mol L^{-1} $NaNO_2$ aqueous solution was used to remove any radiation below 400 nm to ensure that the irradiation of the photocatalytic system occurred only within the range of visible light wavelengths [14].

The photocatalytic reaction was kept at room temperature by a water cool system (Lab Tech Company, USA). The concentration of 4-*t*-OP in each solution was determined by HPLC Shimadzu model LC-9A equipped with a UV detector at 276 nm, and C-18 phenomenex column. The mobile phase was 80% acetonitrile in ultrapure water with a flow rate of 0.8 mL min^{-1}. The UV spectra of 4-*t*-OP solutions were measured on a DR 5000 UV–visible spectroscopy (HACH Corporation, USA).

2.2.2. Characterization of the ~~corroded~~ products

The crystal structure of the ~~corroded~~ products of $NaBiO_3$ was examined by X-ray diffraction (XRD) in the 2θ range 5–55° using Cu-Kα X-ray source ($\lambda = 0.15418$ nm). The transmission electron microscopy (TEM) images were obtained on a JEM 2010 transmission electron microscope. X-ray photoelectron spectroscopic (XPS) characterization was carried out using a PHI-5300 spectrometer. The C 1s ($E = 284.5$ eV) level served as the internal standard. Transmittant ultraviolet–visible light (UV–vis) spectra were obtained by the reflectant spectra conversion based on the Kubelka–Munk method. The spectra were recorded at room temperature on a Hitachi U-3010 spectrophotometer by using $BaSO_4$ as a reference.

3. Results and discussion

3.1. Photocatalytic kinetics experiments

3.1.1. Effect of catalyst dosage

Catalyst dosage is an important parameter in the slurry photocatalytic process. In order to obtain the optimum catalyst dosage, the relationship between the dosage and average reaction rate was investigated as shown in Fig. 1(a). It can be seen that the average reaction rate increased with a dosage up to 0.3125 g L^{-1}, beyond which the average reaction rate became equilibrium. This indicates that the optimal dosage value was 0.3125 g L^{-1} in this experiment, and the measured average photocatalytic removal rate could reach up to 0.0082 mg s^{-1}. When the dosage is less than the optimum value, the catalyst exhibits a lower average reaction rate because there are not enough catalytic active sites to be supplied. However, the average reaction rate begins to be equilibrium if the dosage is much higher than this value. Under such conditions, the light utility efficiency of the Xenon-lamp would not be improved, although the dosage was increased. Chen and Ray [15,16] developed general equations to demonstrate the dependence of degradation rate on the TiO_2 dosage, and the equations can well correlate with the results depicted in Fig. 1(a) for the 4-*t*-OP compound in the $NaBiO_3$ photocatalytic system.

Fig. 1(b) displays the influence of $NaBiO_3$ dosage on the photocatalytic activity. The results clearly show that decomposition under visible light irradiation without catalysts for 1 h was negligibly small, compared with the results obtained in the present of $NaBiO_3$ photocatalysts with different dosages. The maximum removal efficiency after 1 h was around 90% when the optimum dosage was employed. However, the adsorption efficiency of 4-*t*-OP on the surface of $NaBiO_3$ (dosage in the range of 0–0.3125 g L^{-1}) was less than 5% under the same conditions, indicating the high photocatalytic activity of $NaBiO_3$ under visible light irradiation.

3.1.2. Effect of initial 4-*t*-OP concentration

The influence of initial 4-*t*-OP concentration on the photocatalytic rate and apparent rate constant was also investigated, as shown in Fig. 1(c). It is known that the Langmuir–Hinshelwood model is usually used to express the degradation rate descriptions in terms of the removal of compounds or the formation of CO_2. It was found that the photocatalytic degradation of 4-*t*-OP over $NaBiO_3$ was apparently the first-order kinetics model, when the initial 4-*t*-OP concentration was less than 28 ppm. It was noted that when the initial 4-*t*-OP concentration was 56.3 ppm, the first-order kinetics relationship was not pronounced. According to the Langmuir–Hinshelwood model, which ignores the effect of the intermediate product, the photocatalytic reaction rate (r) can be expressed briefly as:

$$r = -\frac{dC}{dt} = K_r \frac{K_a C_0}{1 + K_a C_0}$$

where K_r refers to the apparent rate constant, K_a is the adsorption equilibrium constant and C_0 is the initial concentration. If $K_a C_0 \leq 1$, this expression can be further simplified to:

$$r = K_r K_a C_0$$

This simplified expression suggests that the first-order kinetics will become not important when the initial concentration was high.

On the other hand, apparent rate constant (k) was determined to be 0.01302 min^{-1}, 0.03741 min^{-1}, 0.04462 min^{-1} and 0.0759 min^{-1} for initial concentrations of 4-*t*-OP of 56.3 ppm, 28 ppm, 21.2 ppm and 12.3 ppm, respectively. Thus, the initial concentration was important to the k value of the photocatalytic reaction. The k value can be increased through decreasing the initial 4-*t*-OP concentration. Other authors have reported similar results [17,18] by using different catalysts. It is considered that if the concentration of the organic compound is relative low, $\leq$28 ppm in the present experiment for example, the reaction between the photo-generated hole (or hydroxyl radical •OH) and the compounds determine the whole photocatalytic process. Therefore, the k value increases with the decreasing concentration. What is more, the adsorption performance and the intermediates are also parameters which will influence the kinetic performance [16].

Fig. 1(d) shows the UV spectrum variation of 4-*t*-OP solution with the photocatalytic reaction time. 4-*t*-OP showed two major

Please cite this article in press as: X. Chang, et al., Photocatalytic decomposition of 4-*t*-octylphenol by $NaBiO_3$ driven by visible light: Catalytic kinetic and corroded product characterization, J. Hazard. Mater. (2009), doi:10.1016/j.jhazmat.2009.08.148

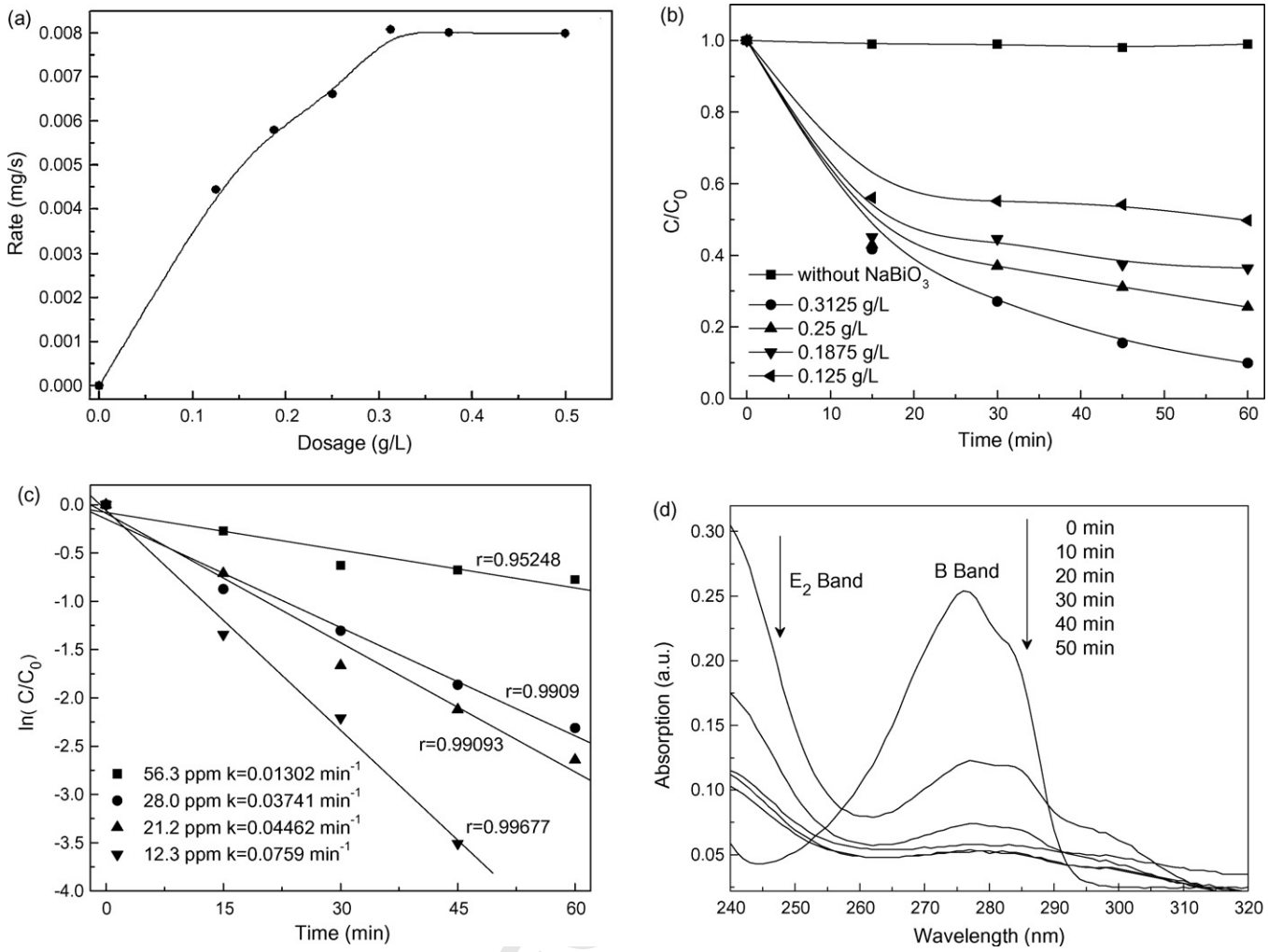

Fig. 1. Effect of catalyst dosage and initial concentration of 4-*t*-OP on the photocatalytic performance: (a) effect of catalyst dosage on the degradation rate of 4-*t*-OP (experimental conditions: pH 7.6–7.7, initial concentration = 29 ppm, and irradiation time = 1 h); (b) effect of catalyst dosage on the concentration change of 4-*t*-OP as a function of time (experimental conditions: pH 7.6–7.7 and initial concentration = 29 ppm); (c) first-order plots for the photocatalytic degradation over $NaBiO_3$ at various initial concentrations (experimental conditions: dosage = 0.3125 g L^{-1} and pH 7.6); and (d) UV absorption spectrum changes of 4-*t*-OP solution (experimental conditions: dosage = 0.3125 g L^{-1}, pH 7.6–7.7, and initial concentration = 29 ppm).

featured absorption bands at 276 nm and 225 nm, corresponding to the E_2 band and B band respectively. It can be found that $NaBiO_3$ photocatalyst can lead to a pronounced decrease in the absorption of E_2 band and B band under the visible light irradiation, and the shape of the absorption peak disappeared after 1 h photocatalysis. In the mean time, the results were further confirmed by HPLC measurement. The HPLC spectrum (not shown in this paper) also revealed that the signal intensity and calculated area of the peak decreased dramatically after 1 h photocatalysis. Some other weak chromatographic signals with different retention times could be observed from the spectrum. The results proved the destruction of the conjugated structure in 4-*t*-OP molecules. A detailed degradation product and pathway are being further studied.

3.1.3. *Effect of initial solution pH*

The pH value of 4-*t*-OP solution is also a key parameter which can affect the photocatalytic process dramatically. The photocatalytic decomposition of 4-*t*-OP by $NaBiO_3$ with different initial pHs is illustrated in Fig. 2(a). The photocatalytic degradation efficiencies were only 55.6% and 57.7% when the initial pH values were 2.13 and 11.94, respectively. In the pH range of 2–12, it was found the highest photocatalytic activity could be acquired when the pH value was closed to neutral condition. In this series of experiments, the maximum removal rate was 90.1% when the initial pH was 7.9. The result reveals that if the initial pH value is over acid or basic, the photocatalytic activity can be suppressed and the decreasing rate of removal efficiency will be higher with increases in the concentrations of H^+ ($[H^+]$) and OH^- ($[OH^-]$).

In order to study the reason why photocatalytic activity is low at relatively high $[OH^-]$, the effect of pH value on the adsorption of 4-*t*-OP on the surface of $NaBiO_3$ (Fig. 2(b)) was performed in an incubator shaker. The tracing of pH value of the 4-*t*-OP solution with the photocatalytic process (Fig. 2(c)) was also investigated. It is found in Fig. 2(b) that the adsorption performance over $NaBiO_3$ material became weaker when increasing the initial pH value of 4-*t*-OP solution in the range of 8–13, and there was almost no adsorption interaction when pH was 12.6. It is known that the main steps of the photocatalytic process take place on the surface of the photocatalyst, according to the principle of the photocatalytic process. The adsorption of organic compounds on the photocatalyst surface can affect the photocatalytic process, and usually high adsorption capacity is favored [19]. Therefore, the weak adsorption may lead to a low photocatalytic performance under basic solution. Meanwhile, it is noted that the pH value of the 4-*t*-OP solution increased from ~7.7 to ~11.0 after 1 h photocatalytic reaction, and thus the process of OH^- forming during the photocatalysis indicates

Please cite this article in press as: X. Chang, et al., Photocatalytic decomposition of 4-*t*-octylphenol by $NaBiO_3$ driven by visible light: Catalytic kinetic and corroded product characterization, J. Hazard. Mater. (2009), doi:10.1016/j.jhazmat.2009.08.148

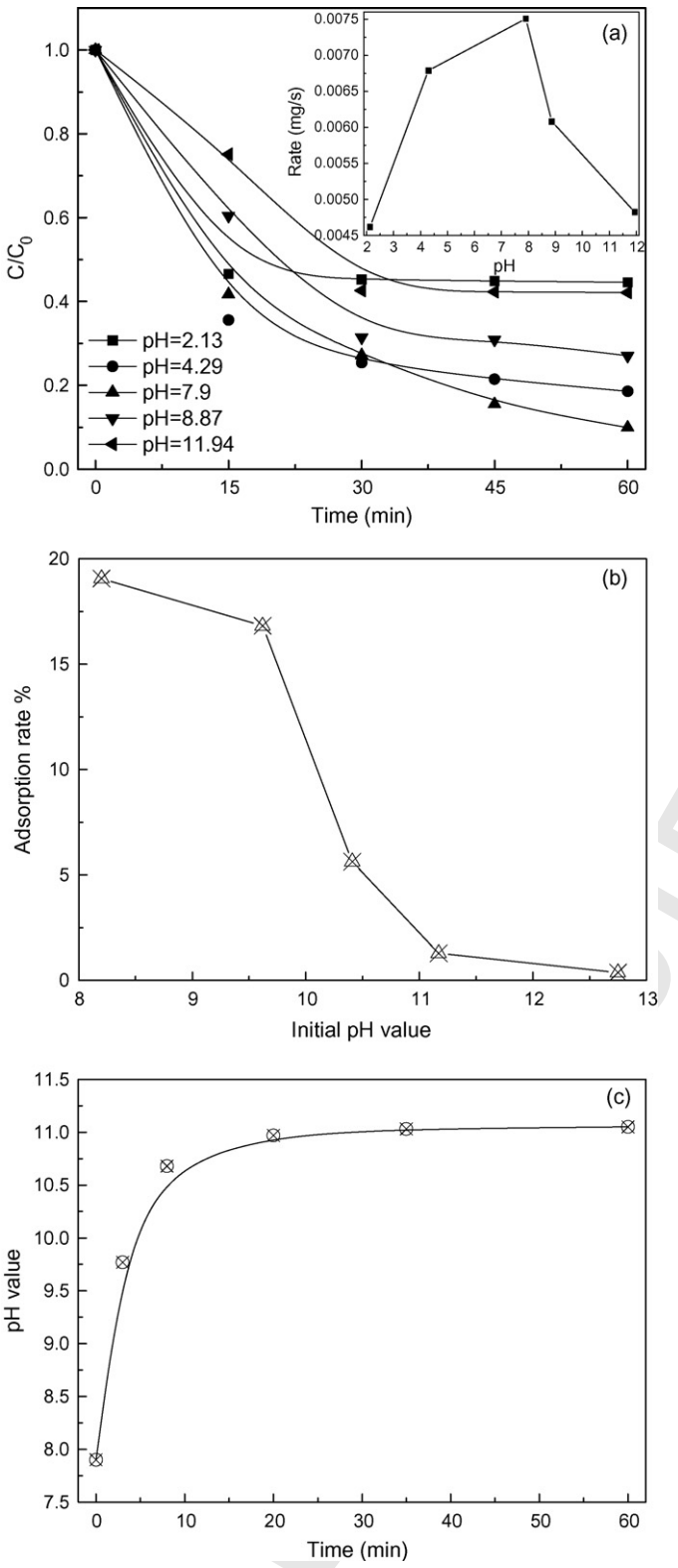

Fig. 2. Influence of pH of the 4-*t*-OP solution on the photocatalytic performance: (a) influence of pH of the 4-*t*-OP solution on the concentration change of 4-*t*-OP as a function of time, inset: the changes of average catalytic reaction rate at various pHs (experimental conditions: dosage = 0.3125 g L^{-1} and initial concentration = 29–31 ppm) and (b) influence of pH value on the adsorption of 4-*t*-OP on the surface of $NaBiO_3$ after 1 h shaking (experimental conditions: temperature = 25 ± 2 °C and rotational speed = 150–155 rpm); and (c) changes of pH value as a function of irradiation time (experimental conditions: dosage = 0.3125 g L^{-1}, pH 7.7, and initial concentration = 29 ppm).

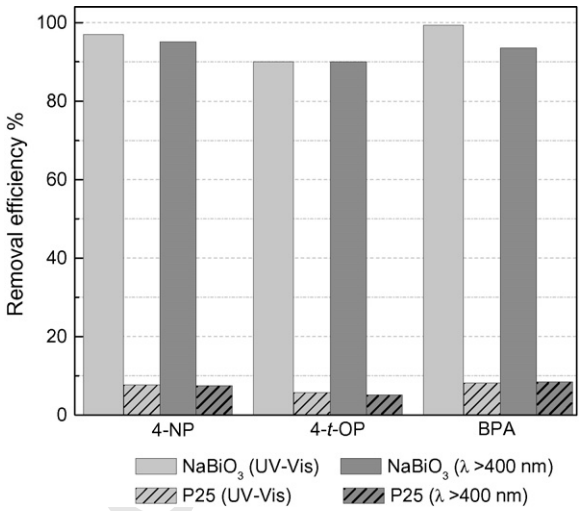

Fig. 3. Photocatalytic degradation results of three kinds of typical EDCs (4-NP, 4-*t*-OP and BPA) comparison between $NaBiO_3$ and P25 (experimental conditions: dosage = 0.3125 g L^{-1}, pH 7.6–7.9, initial concentration = 29–31 ppm, and irradiation time = 1 h).

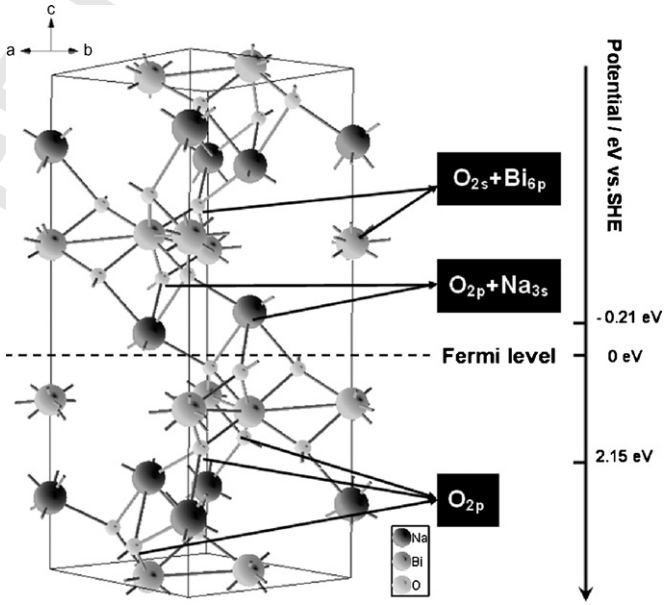

Fig. 4. Schematic band structure of $NaBiO_3$.

that the reaction is suppressed when the pH value of the 4-*t*-OP solution is under the basic solution environment.

3.1.4. Photocatalytic activity comparison between $NaBiO_3$ and P25

$NaBiO_3$ exhibited an extremely efficient photocatalytic performance (removal efficiency is over 90%) towards three types of typical EDCs, i.e. 4-nonylphenol (4-NP), bisphenol-A (BPA) and 4-*t*-OP under visible light or Xenon-lamp irradiation, compared to the conventional and commercialized photocatalyst P25, as illustrated in Fig. 3. The nano-sized TiO_2 (P25) showed very low removal efficiency (removal efficiency is less than 9%) for the reason that it is only sensitive to UV and the removal efficiency may be attributed to the adsorption behavior and weak photocatalytic reaction over P25 under Xenon-light irradiation. The CB and VB edges for the bulk phase $NaBiO_3$ material were calculated on the basis of the atom's

Please cite this article in press as: X. Chang, et al., Photocatalytic decomposition of 4-*t*-octylphenol by $NaBiO_3$ driven by visible light: Catalytic kinetic and corroded product characterization, J. Hazard. Mater. (2009), doi:10.1016/j.jhazmat.2009.08.148

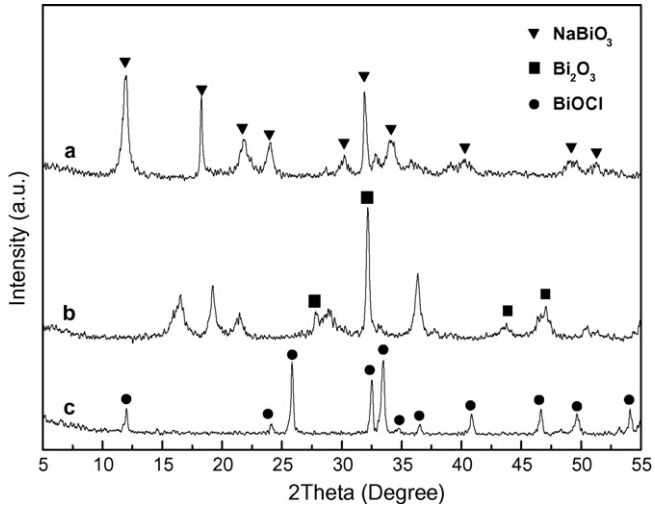

Fig. 5. XRD patterns of the products at different initial 4-*t*-OP aqueous pH values: (a) pH 7.9; (b) pH 4.29; and (c) pH 2.13.

Mulliken electronegativity, the expression of which is:

$$E_{CB} = X - E^c - \frac{1}{2}E_g$$

where X is the absolute electronegativity of semiconductor; E^c is the energy of free electrons on hydrogen scale (≈4.5 eV) and E_g is the band gap of semiconductor. The calculated result shows that the CB and VB edges for $NaBiO_3$ semiconductor were −0.21 eV and 2.15 eV, respectively. A schematic band structure of $NaBiO_3$ was made based on the calculated CB and VB edges and the density of states (DOS) distribution [12] (Fig. 4). It should be noted that $NaBiO_3$ has a very interesting energy band structure. The hybridized sp orbital at the bottom of CB (Na 3s and O 2p hybridized orbits) could support a high mobility on the sp bands for the photo-excited electrons, which may lead to the suppression of electron–hole pair recombination, and a relatively higher photocatalytic activity of the material than that of any other photocatalysts [12].

3.2. The microstructure analysis of the ~~corroded~~ product

3.2.1. XRD analysis

The reason why $NaBiO_3$ exhibited low photocatalytic activity is because the catalyst is corroded under acid condition, which can be visually observed from the color changes of the yellow-colored $NaBiO_3$. The XRD characterization was employed to investigate the crystal structure changes of the photocatalyst after photocatalytic reaction at different acid conditions. The XRD patterns of the products at different initial pH values of 4-*t*-OP aqueous are shown in Fig. 5. It is found that all diffraction peaks can be indexed to the

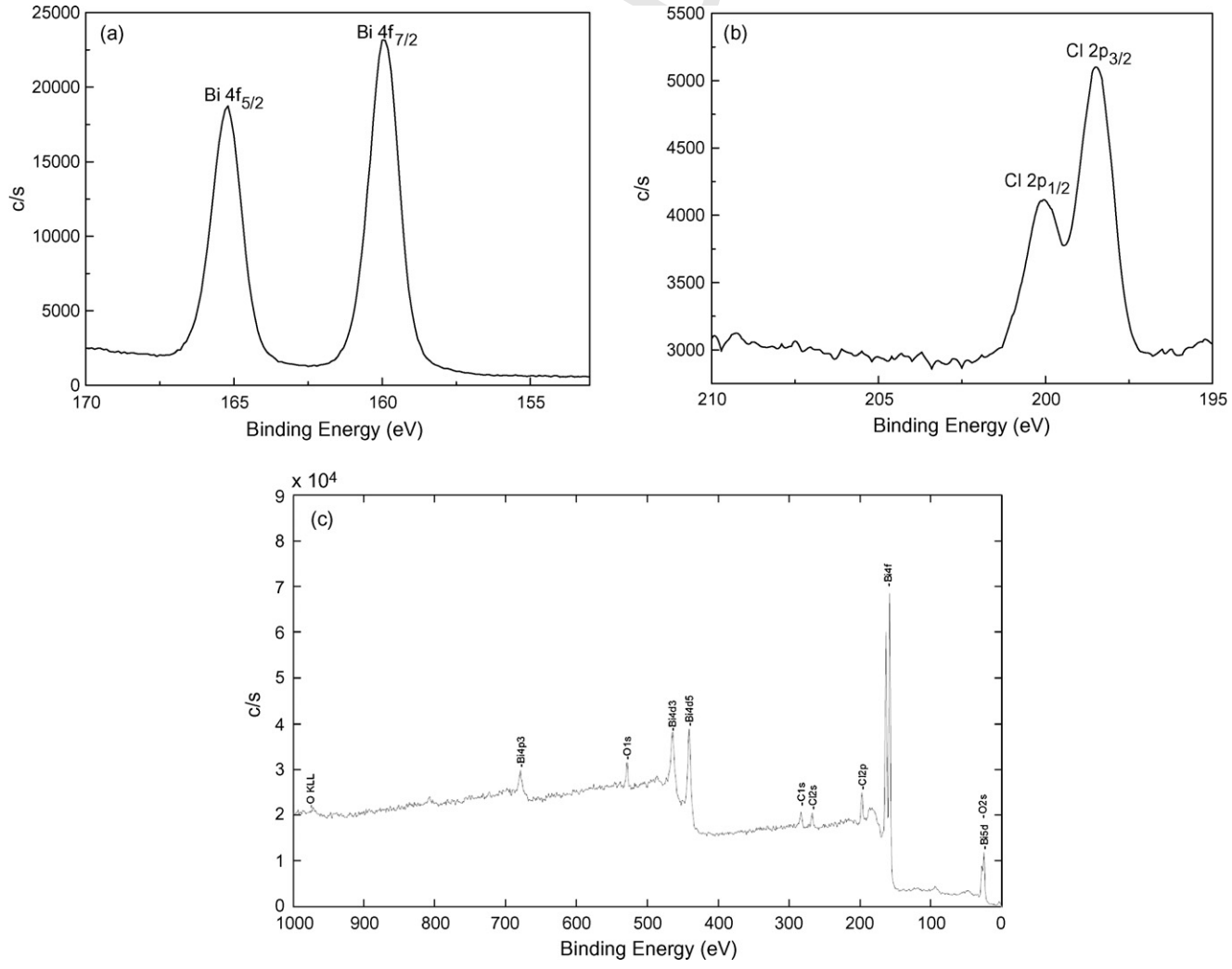

Fig. 6. High resolution XPS of Cl 2p (a) and Bi 4f (b) levels in BiOCl and (c) low resolution XPS of the sample.

Please cite this article in press as: X. Chang, et al., Photocatalytic decomposition of 4-*t*-octylphenol by $NaBiO_3$ driven by visible light: Catalytic kinetic and corroded product characterization, J. Hazard. Mater. (2009), doi:10.1016/j.jhazmat.2009.08.148

hexagonal structure of $NaBiO_3$ (JCPDS card 30-1161) with fine crystallinity after photocatalytic reaction at an initial 4-*t*-OP aqueous pH of 7.9. Three strongest diffraction peaks were observed at 2θ of 11.944°, 18.272°, and 31.935°, which correspond to the crystal indexes of (0 0 1), (1 0 0) and (1 1 0). However, when the initial 4-*t*-OP aqueous pH was less than 7, an obvious corrosion took place. Some Bi_2O_3 diffraction peaks (JCPDS card 74-1373) were observed if the initial pH was 4.29. When the initial pH was 2.13, the color of ~~corroded~~ products became white, and the XRD analysis indicated that the white-colored products was BiOCl (JCPDS card 82-0485).

3.2.2. XPS analysis

XPS analysis was used to further confirm the valence state of bismuth and chloride element in the ~~corroded~~ sample. Fig. 6 shows the low resolution XPS graph of the ~~corroded~~ sample. The XPS analysis indicated that the sample consisted of bismuth, oxygen and chloride elements. Fig. 6(a) and (b) shows the high resolution XPS of Cl 2p and Bi 4f level for the BiOCl sample. It can be observed that the spin–orbit splitting peaks of Cl 2p and Bi 4f level are in accordance with the following law:

$$J = |L \pm Se|$$

where J is the inner quantum number of the interaction between the spin and orbit, L and Se is the azimuthal quantum number and spin quantum number. In Fig. 6(b), the peaks at 165.2 eV and 159.9 eV, corresponding to the binding energies of Bi $4f_{5/2}$ and Bi $4f_{7/2}$, demonstrate that the main chemical states of bismuth in the ~~corroded~~ samples were trivalence [20].

On the other hand, the Cl 2p peak, shown in Fig. 6(a), is splitted into two peaks (200.2 eV and 198.2 eV), which can be assigned to the Cl $2p_{3/2}$ and Cl $2p_{1/2}$, respectively, further confirming the BiOCl material was formed during the photocatalytic process.

3.2.3. TEM analysis

TEM analysis was employed in this experiment to observe the morphology and to confirm the crystal growth direction of the ~~corroded~~ product. Fig. 7(a) shows the TEM image of BiOCl grains, indicating that the grain size of the samples was in the range of 150–180 nm. Fig. 7(b) and (c) gives the selected area electron diffraction (SAED) patterns of region A and B. It is found that the SAED patterns are different from the changes of the selected area. The SAED patterns of region A and B were polycrystalline and single crystalline. In the meantime, from the SAED pattern of Fig. 7(b), it was estimated that the radius ratio of the three Debye–Scherrer rings were $R_1^2:R_2^2:R_3^2 = 1:2:4$, indicating the tetragonal crystallography of the sample.

3.2.4. UV–vis transmittance spectra analysis

BiOCl material is also a UV-responded photocatalyst which has been previously reported [21–24]. The transmittance spectra of $NaBiO_3$ and its ~~corroded~~ product BiOCl materials are shown in Fig. 8. The optical absorptions of the powders started at about 457 nm and 372 nm, corresponding to the absorption edges of $NaBiO_3$ and BiOCl, respectively. The spectra were used to determine the optical properties of the samples. According to the equation:

$$\alpha E_{photon} = K(E_{photon} - E_g)^n$$

where α is the absorption photon coefficient, E_{photon} is the discrete photon energy, K is a constant, and E_g is the band gap energy, and n depends on the type of optical transition in the gap region. n is 1/2, 3/2, 2 or 3 for transitions being direct and allowed, direct and forbidden, indirect and allowed, and indirect and forbidden [25,26]. According to Ref. [27], both the values of n for $NaBiO_3$ and BiOCl were determined to be 2, and the results were in agreement with the previous studies [13,23]. A classical Tauc approach is employed to evaluate the band gap of the samples (inset of Fig. 8). The extrapolated value (the straight lines to the x axis) of E at $x = 0$ gives the adsorption edge energies corresponding to $E_g = 2.36$ and 3.28 eV, for $NaBiO_3$ and BiOCl. It is not easy to understand that the yellow-colored $NaBiO_3$ catalyst can absorb a part of the visible light but the white-colored BiOCl product cannot. Meanwhile, the Commission International de L'Eclairage (CIE) coordinates (illustrated in Fig. 9) based on the UV–vis transmittance spectrum of $NaBiO_3$ and BiOCl are calculated to be (0.4809, 0.4102) and (0.3304, 0.3341), respectively.

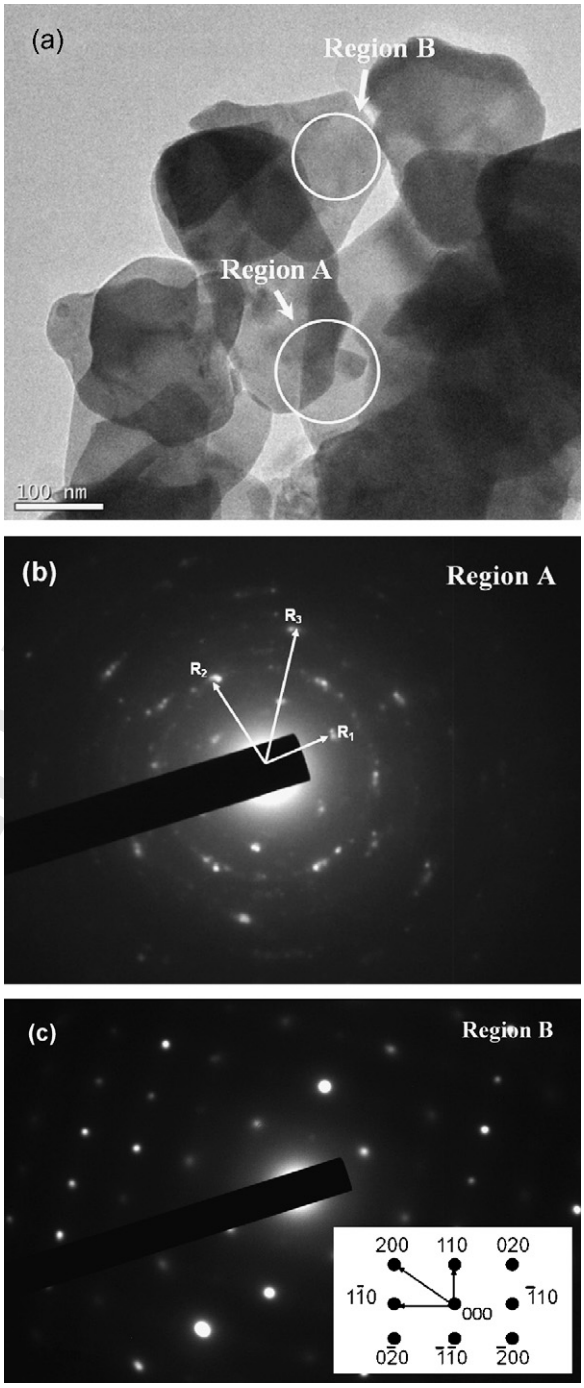

Fig. 7. TEM and SAED results of the ~~corroded~~ product BiOCl: (a) TEM image of BiOCl grains and (b and c) SAED of region A and B in (a) (inset of (c) presents the indexing results).

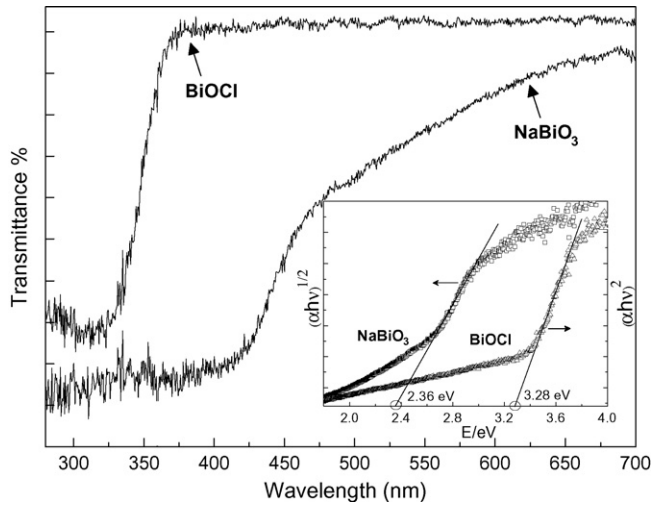

Fig. 8. UV–vis transmittance spectrum of $NaBiO_3$ and BiOCl semiconductors (inset: calculation diagrams of their band gap).

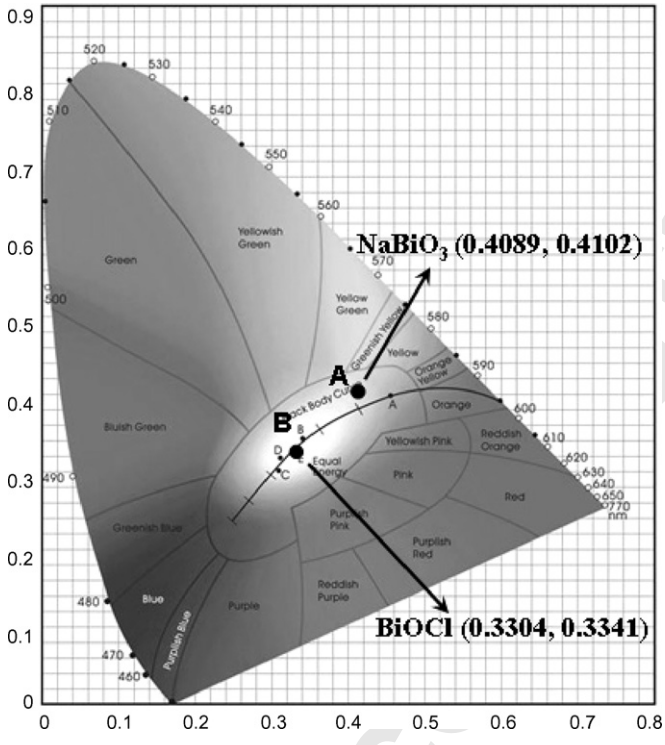

Fig. 9. CIE coordinates of $NaBiO_3$ (point A) and BiOCl (point B) semiconductors.

In summary, the formation of BiOCl material after corrosion at acid condition via the systematic microstructure characterizations is ascertained. The result is interesting and may support a new strategy to obtain BiOX (X = Cl, Br, I) materials via the Bi^{5+} to Bi^{3+} oxidation–reduction approach. However, most of the previous studies on fabrication of BiOX (X = Cl, Br, I) are on the basis of Bi^{3+} hydrolysis reaction [21–24,28] and the detailed study on this reaction process is being further investigated.

4. Conclusions

This study reports the photocatalytic removal activity of 4-*t*-OP over $NaBiO_3$ catalyst under the visible light irradiation. It is found that the catalyst dosage, initial 4-*t*-OP concentration and the pH value of the solution can affect the photocatalytic performance and kinetics greatly. The photocatalyst presents an excellent photocatalytic activity compared to commercialized TiO_2 photocatalyst (P25). However, it should be noted that such catalyst was not stable under acidic conditions, and it can convert into BiOCl or other Bi^{3+} containing compounds in the presence of hydrochloric acid aqueous solution. Thus, this unstable feature of $NaBiO_3$ may block its further application on photocatalysis.

Acknowledgments

This research was financially supported by National Natural Science Foundation of China (No. 50538090), National Science Fund for Distinguished Young Scholars of China (No. 50625823), and National Key Project of Scientific and Technical Supporting Programs (No. 2007BAC03A09).

References

[1] T. Tsuda, A. Takino, M. Kojima, H. Harada, K. Muraki, M. Tsuji, 4-Nonylphenols and 4-tert-octylphenol in water and fish from rivers flowing into Lake Biwa, Chemosphere 41 (2000) 757–762.
[2] G. Renata, F. Anna, B. Bogusław, A bio-imprinted urease biosensor: improved thermal and operational stabilities, Talanta 74 (2008) 655–660.
[3] K. Inumaru, M. Murashima, T. Kasahara, S. Yamanaka, Enhanced photocatalytic decomposition of 4-nonylphenol by surface-organografted TiO_2: a combination of molecular selective adsorption and photocatalysis, Appl. Catal. B: Environ. 52 (2004) 275–280.
[4] W.-T. Tsai, et al., Photodegradation of bisphenol-A in a batch TiO_2 suspension reactor, J. Hazard. Mater. (2009), doi:10.1016/j.jhazmat.2009.02.034. Q1
[5] R. Wang, D. Ren, S. Xia, Y. Zhang, J. Zhao, Photocatalytic degradation of bisphenol A (BPA) using immobilized TiO_2 and UV illumination in a horizontal circulating bed photocatalytic reactor (HCBPR), J. Hazard. Mater. (2008), doi:10.1016/j.jhazmat.2009.04.036.
[6] S. Yamazakia, T. Moria, T. Katoua, M. Sugiharaa, A. Saekia, T. Tanimurab, Photocatalytic degradation of 4-tert-octylphenol in water and the effect of peroxydisulfate as additives, J. Photochem. Photobiol. A: Chem. 199 (2008) 330–335.
[7] G. Blasse, G.J. Dirksen, P.H.M. Korte, Materials with cationic valence and conduction bands for photoelectrolysis of water, Mater. Res. Bull. 16 (1981) 991–998.
[8] N. Lakshminarasimhan, Y. Park, W. Choi, Role of valency ordering on the visible light photocatalytic activity of $BaBi_{0.5}{}^{3+}Bi_{0.5}{}^{5+}O_3$, Chem. Phys. Lett. 452 (2008) 264–268.
[9] J. Tang, Z. Zou, J. Ye, Efficient photocatalytic decomposition of organic contaminants over $CaBi_2O_4$ under visible-light irradiation, Angew. Chem. Int. Ed. 43 (2004) 4463–4466.
[10] J. Tang, Z. Zou, J. Ye, Photocatalytic decomposition of organic contaminants by Bi_2WO_6 under visible light irradiation, Catal. Lett. 92 (2004) 53–56.
[11] C. Zhang, Y. Zhu, Synthesis of square Bi_2WO_6 nanoplates as high-activity visible-light-driven photocatalysts, Chem. Mater. 17 (2005) 3537–3545.
[12] T. Kako, Z. Zou, M. Katagiri, J. Ye, Decomposition of organic compounds over $NaBiO_3$ under visible light irradiation, Chem. Mater. 19 (2007) 198–202.
[13] J. Kou, H. Zhang, Z. Li, S. Ouyang, J. Ye, Z. Zou, Photooxidation of polycyclic aromatic hydrocarbons over $NaBiO_3$ under visible light irradiation, Catal. Lett. 122 (2008) ~~(2008)~~ 131–137.
[14] H. Xia, H. Zhuang, T. Zhang, D. Xiao, Photocatalytic degradation of Acid Blue 62 over CuO–SnO_2 nanocomposite photocatalyst under simulated sunlight, J. Environ. Sci. 19 (2007) 1141–1145.
[15] D.W. Chen, A.K. Ray, Photodegradation kinetics of 4-nitrophenol in TiO_2 suspension, Water Res. 32 (1998) 3223–3234.
[16] D.W. Chen, A.K. Ray, Photocatalytic kinetics of phenol and its derivatives over UV irradiated TiO_2, Appl. Catal. B: Environ. 23 (1999) 143–157.
[17] Y. Inel, A. Okte, Photocatalytic degradation of malonic acid in aqueous suspensions of titanium dioxide: an initial kinetic investigation of CO_2 photogeneration, J. Photochem. Photobiol. A: Chem. 96 (1996) 175–180.
[18] H. Fu, C. Pan, W. Yao, Y. Zhu, Visible-light-induced degradation of Rhodamine B by nanosized Bi_2WO_6, J. Phys. Chem. B 109 (2005) 22432–22439.
[19] C. Minero, F. Catozzo, E. Pelizzetti, Role of adsorption in photocatalyzed reactions of organic molecules in aqueous titania suspensions, Langmuir 8 (1992) 481–486.
[20] W.E. Morgan, W.J. Stec, J.R. Vanwazer, Inner-orbital binding-energy shifts of antimony and bismuth compounds, Inorg. Chem. 12 (1973) 953–955.
[21] H. An, Y. Du, T. Wang, C. Wang, W. Hao, J. Zhang, Photocatalytic properties of BiOX (X = Cl, Br, and I), Rare Metals 27 (2008) 243–250.
[22] C. Wang, C. Shao, Y. Liu, L. Zhang, Photocatalytic properties BiOCl and Bi_2O_3 nanofibers, Scripta Mater. 59 (2008) 332–335.
[23] K. Zhang, C. Liu, F. Huang, C. Zheng, W. Wang, Study of the electronic structure and photocatalytic activity, Appl. Catal. B: Environ. 68 (2006) 125–129.
[24] X. Zhang, Z. Ai, F. Jia, L. Zhang, Generalized one-pot synthesis, characterization, and photocatalytic activity of hierarchical BiOX (X = Cl, Br, I) nanoplate microspheres, J. Phys. Chem. C 112 (2008) 747–753.

[25] A. Hjelm, C. Granqvist, Electronic structure and optical properties of WO_3, $LiWO_3$, $NaWO_3$, and HWO_3, Phys. Rev. B 54 (1996) 2346–2445.
[26] G. Li, T. Kako, D. Wang, Z. Zou, J. Ye, Composition dependence of the photophysical and photocatalytic properties of $(AgNbO_3)_{1-x}(NaNbO_3)_x$ solid solutions, J. Solid State Chem. 180 (2007) 2845–2850.
[27] J. Tang, Z. Zou, J. Ye, Photophysical and photocatalytic properties of $AgInW_2O_8$, J. Phys. Chem. B 107 (2003) 14265–14269.
[28] J. Henle, P. Simon, A. Frenzel, S. Scholz, S. Kaskel, Nanosized BiOX (X = Cl, Br, I) particles synthesized in reverse microemulsions, Chem. Mater. 19 (2007) 366–373.

Please cite this article in press as: X. Chang, et al., Photocatalytic decomposition of 4-*t*-octylphenol by $NaBiO_3$ driven by visible light: Catalytic kinetic and corroded product characterization, J. Hazard. Mater. (2009), doi:10.1016/j.jhazmat.2009.08.148